Archives of Civil and Mechanical Engineering (2022) 22:174
https://doi.org/10.1007/s43452-022-00495-5

ORIGINAL ARTICLE

Performance of steel–polymer–steel seafloor pipeline buried in earthquake fault zones

Vul Thang[1] · David Hui[1] · Peter W. Marshall[2] · Jianren Zhou[3]

Received: 27 November 2021 / Revised: 25 June 2022 / Accepted: 10 July 2022 / Published online: 29 July 2022

Abstract

Steel tubular structures are widely used in offshore structures, such as fixed, floating, and seafloor pipelines. The earthquake can cause relatively large pipe displacement, especially in the fault zone. Therefore, single-wall buried pipelines or piles of the offshore fixed platform in these zones could be under buckling and wrinkling which would lead to the severely deteriorated performance of the pipelines or costly failure. The purpose of this research is to prevent these types of failures by developing innovative double-wall steel–polymer–steel (SPS) composite pipes in place of single-wall pipes. In the double-wall pipe, the annulus of the inner and outer pipe was grouted with polymer. Verification exercises for single-wall pipe in air and buried in clay, and double-wall pipes in the air were performed. Thereafter, an analysis of laterally loaded SPS double-wall composite pipes in clay was performed and the pipe responses were examined. A comparison of performance behaviors for single and double-wall pipes was also performed. It was found from this research that double-wall SPS composite pipes demonstrated increased tolerance for higher levels of displacements, strain, stress, and ovality under work environments where pipelines could be subjected to large displacement in the earthquake fault zone. For those composite pipes in which there is no bond between the polymer layer and inner/outer steel pipes, the composite pipes showed wrinkles on the compression side of the pipe even under a small displacement. So, the polymer and steel must be bonded to have a good composite section. The composite pipes with stiffer polymer grout showed a better performance while soft polymer did not contribute to the overall stiffness of the composite pipes. In addition, the effects of weld on the outer steel pipes were also studied and the results were documented.

Keywords Steel–polymer–steel · Sandwich pipe · Composite pipe · Sandwich pipe · Pipeline · Strain-based design · Pipe ovalization

1 Introduction

Buried pipelines in earthquake fault zone can experience large displacement. Figure 1 shows the problem of a pipeline crossing a strike-slip fault. It is similar to piling crossing a ground slip plane. In hard rock, the pipeline trench would be backfilled with softer soil, e.g., medium clay having a compressive strength, 2c, of 58 kPa (1200 psf). The cohesion of the clay is denoted as c. Soil flowing around the pipe with diameter D develops an ultimate transverse loading per unit length of Q = 12 cD. Compared to the expected pipe movement, the deflection required for the soil to reach ultimate is small, so its behavior is assumed to be rigid plastic [1]. The issue with the single-wall pipe is that wrinkles develop in the pipe when the pipe experiences large displacement or bending. The wrinkles in the pipeline can significantly reduce the pipe opening and can obstruct the pigging device. In

✉ Vul Thang
vulthang@gmail.com

David Hui
dhui@uno.edu

Peter W. Marshall
mhpsyseng@gmail.com

Jianren Zhou
jizhou@pvamu.edu

[1] Department of Mechanical Engineering, University of New Orleans, New Orleans, LA 70148, USA

[2] Moonshine Hill Propriety, 2115 Winchester Blvd, Campbell, CA 95008, USA

[3] Department of Mechanical Engineering, Prairie View A&M University, P.O.Box 519; MS 2525, Prairie View, TX 77446, USA

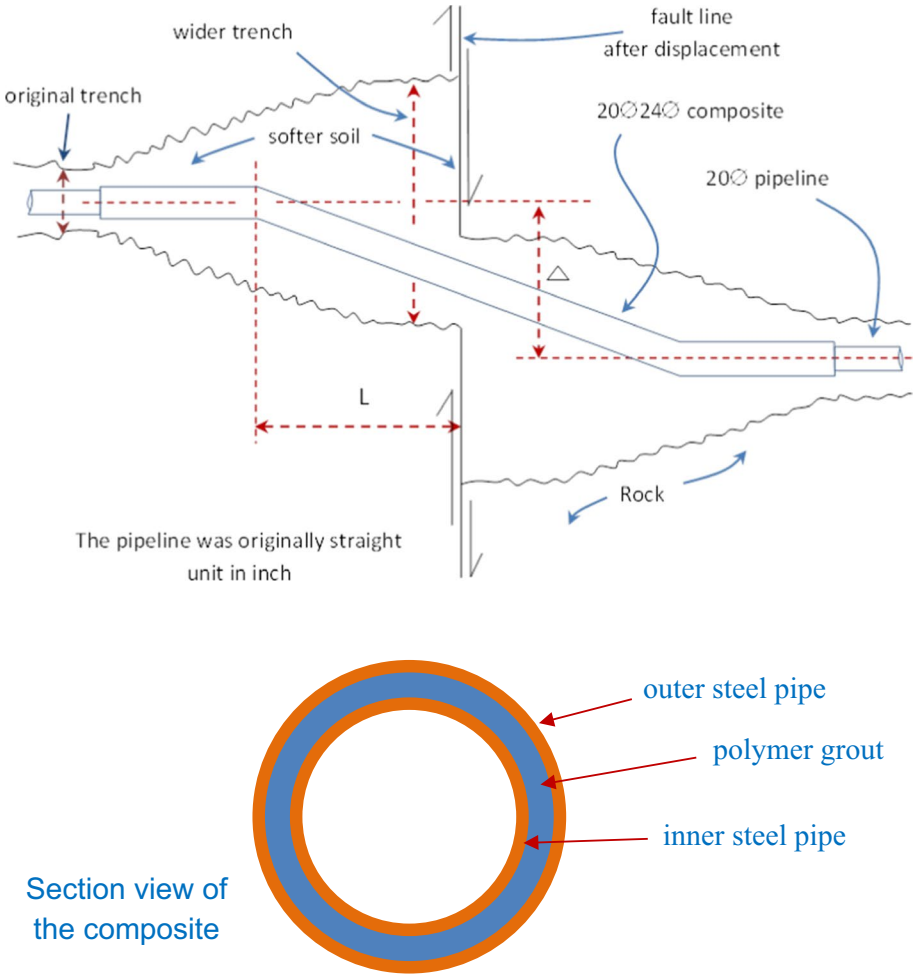

Fig. 1 Exemplary displacement due to earthquake [2], and section view of the composite pipe

addition, the wrinkles can also increase the stress and strain on the pipe, and this aid pipeline failure. Thang, Marshall, and Hui [2] including several researchers performed studies to improve wrinkles in the pipe [3–5]. Pipeline failures especially in the oil and gas industry have caused significant losses.

Double-wall pipes with annulus grouted with cement, and concentric tubular have been used as oil well casing since the late 1800s, and the composite section has also been used with piles in offshore jacket platform legs. There is a bonding issue for the cement grouted composite section, disbonding between cement and the steel surfaces, which reduces the effectiveness of the composite section.

The earthquake may be associated with ground distortion of several meters or feet slip (delta) as shown in Fig. 1. This can produce severe elastic stresses in piling, conductors, and pipelines. However, if there is sufficient ductility, the displacements can safely be accommodated in the plastic range [6]. Figure 1 drawn represents pipeline displacement failure due to an earthquake at the fault zone and section view of the double-wall composite pipe. Due to large displacement, the pipeline may buckle, forming a hinge, and have sharp slope discontinuity on the pipe which eventually may appear linear. However, depending on the displacement due to the earthquake, the pipe may bend and form such as the 'S' shape which is nonlinear. This research study is referring to pipeline displacement caused by the earthquake fault.

Recently, there were several studies conducted to increase the steel to cement grout bond [7–20], and specific and individual citations of these researchers' work are included in Sect. 3. Thang et al. [21] conducted research on the studded bond between steel–concrete–steel sandwich shells using mixtures of steel and synthetic fibers with cement in the grout for offshore structure applications. In large shell structures, a plain concrete–steel interface often disbonds due to shrinkage, no stress is required. All that is left is contact friction. The studded bond surfaces were found to develop $0.035f'_c$ in peel-off tension, and $0.084f'_c$ in shear, for concrete with compressive strength $f'_c = 68{,}900$ kPa (10,000 psi). In this research work, pipelines are analyzed as structural members. The polymer grout and steel surface are assumed perfectly bonded due to epoxy-like adhesion between the two materials, and the large strain tolerance of

polymers. Thus, there is no deboning within the composite section.

In this research, first, FE analysis verification exercises were performed for pipes in air and pipe embedded in clay for the single and double-wall composite pipes. Combing two asymmetric pipes in clay, a pipeline is obtained. Second, FE analyses for single-wall tubular were performed in clay. Then, further FE analyses were performed on polymer grouted double-wall composite section and the results were compared against available literature, and new findings were documented.

2 Verification of laterally loaded pipe in clay

Matlock [22] performed laterally loaded pipe in soft clay, near the mouth of the Sabine River. The clay's vane shear strength was 14.4 kPa (300 psf). In this research work, FE analyses were performed using 2 methods. Then, they were compared with the test results. The first method used was the modified Drucker–Prager cap model [23]. The second method was Marshall's unpublished method plastic clay model. Abaqus 6.14 user manual [23] and Helwany [24] were used in modeling the pipeline in clay. Abaqus manual [23] contains information using Drucker–Prager cap modeling and Helwany [24] provided some examples of modeling laterally loaded piles in clay.

The clay unit weight was taken as 20 kN/m^3. The modulus of elasticity of the clay was taken as 2150 kPa. This value was used because E_c/c was taken as 150. The value of the modulus of elasticity ranges from 50 to 200 [22]. The pipe diameter was 31.9 cm and the wall thickness was 1.27 cm. The pipe embedded length in the clay was 12.8 m (40 ft). Figure 2 shows the clay FE model with pipe embedded in it, boundary conditions, and meshes. The pipe stick-out was 6.36 mm. Lateral displacement was applied at the pipe top. The base was pinned. The sides were restrained against lateral movement. The soil top surface was restrained against Y direction, modeled as if the fault plane was slick and soil was not allowed to cross it. The pipe and clay interface was a separable contact surface with friction. Displacement controlled load was applied laterally at the top of the pipe until the pipe yielded to the ultimate limit strength.

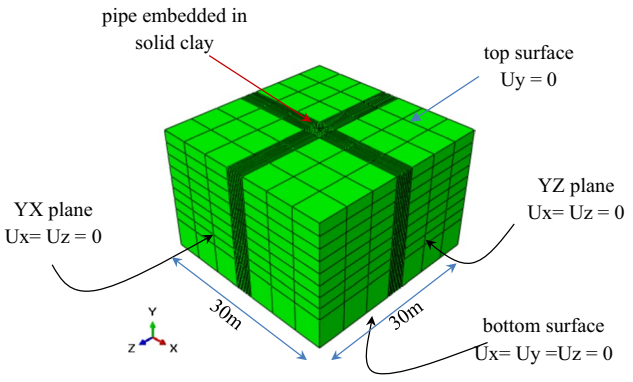

Fig. 2 Meshed model of pipe and clay with the boundary conditions [25]

2.1 Material properties

For the cap model, the strain value (ε) of the clay was taken as 0.02 for ε_{50} and 0.06 for $3\varepsilon_{50}$. Cap plasticity and cap hardening parameters are shown in Table 1. The cap hardening input used was similar to the plastic stress–strain curve used for Marshall's plastic model, but the strain values used are different.

Yield stress and the plastic strain in the cap hardening were entered for the cap plasticity. The stress–strain curves used for the clay and steel are shown in Fig. 3. The strain value used is widely accepted by several papers and the soil mechanics books, including Matlock [22]. The strain value for very soft clay is 0.02. The clay cohesion from the Sabine River mouth's test was 14.4 kPa (300 psf).

For Marshall's plastic model, the strain value of the clay was taken as 0.005 for ε_{50} and 0.015 for $3\varepsilon_{50}$. The compressive strength of the clay was the same as that of Matlock's Sabine clay, 28.8 kPa. The cap hardening stress–strain and plastic stress–strain curves used for cap plasticity and Marshall's plastic model are shown in Fig. 3.

Steel Modulus of Elasticity was taken as 200,000,000 kPa and Poisson's ratio was 0.3. Clay elastic modulus was 7000 kPa and Poisson's ratio was 0.4. This soil was a medium clay model used in Marshall [26].

2.2 Pipe ovalization

Buried pipeline plastic ovalization should be limited as excessive ovalization could hinder the passage of devices in the pipe such as pigging. Ovalization can also cause large strain in plastic which can eventually cause a fracture. In addition, large out-of-roundness can cause issues with girth welding. Different codes provide different ovality calculations and limits. API RP 1111 [27] gives ovality limit, δ, as:

Table 1 Clay parameter input for cap plasticity model [25]

Elastic modulus (kPa)	2150
Poisson's ratio	0.4
Angle of friction (degrees)	20
Cap eccentricity	0.1
Initial yield surface	0
Transition surface radius	0
Flow stress ratio	1.0

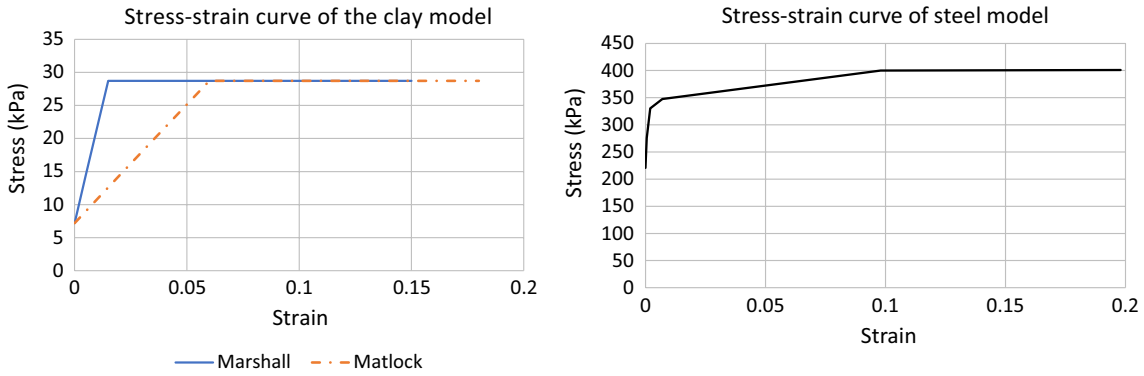

Fig. 3 Stress–strain curve for the plastic clay model and the steel [25]

$$\Delta = \frac{D_{max} - D_{min}}{D_{max} + D_{min}}$$

where

D_{max} = the maximum diameter at any given cross-section.

D_{min} = the minimum diameter at any given cross-section.

API Specification 5L [28] provided a pipe out-of-roundness design limit. As per the specification provided, out-of-roundness for pipe except end is 2% and pipe end is 1.5% for pipe diameter 50.8 cm (20 in.). The ovality issue occurs within the pipe, not the end. Thus, the larger ovality of 2% is applicable.

Fatigue and fracture of the pipeline can be a major concern where the pipeline experiences free span vortex-induced vibration and cyclic thermal loading [29]. Mohr [30] mentioned that pipe bend testing results show buckles on the compression side rather than fractures. Thus, for now, this research paper will focus on the bending, strain, and ovalizing of the pipeline.

Ovality limit stated in DNV-OS-F101 [30], f_0, is:

$$f_0 = \frac{D_{max} - D_{min}}{D}$$

Strain limit is taken as 2% [31, 32]. Liu, Liu, and Zhang [33] provided a summary of ovalization limit acceptance by the industries as shown in Table 2.

The welding effect on the outer pipe in the areas of stress, strain, ovality, and force–displacement was also studied. The weld connection was modeled in the FE beam as per API 579–1/ASME FFS-1 [34].

3 Steel–concrete-steel double-wall pipe

Double-wall composite, steel–concrete–steel tubular axial loading has been widely studied by many researchers. Tao, Han, and Zhao [7] also performed several concretes filled double skin steel tubular stub column tests and some of the test results are used to validate ABAQUS finite element analysis results in this research. Hu and Su [8], Pagoulatou et al. [9], and Liang [10] also performed FE analysis on concrete-filled double-wall steel tubular stub columns.

Table 2 Pipeline ovalization limit [33]

Criteria	Ovalization Limit/%
CSA-Z662-07 App.C	3.0 (6.0)[a]
DNV-OS-F101 (2000)	3.0
API 1111-1999	5.5–6.2
Murray et al. (Murray and Bilston 1992)	4.3–6.5[b]

[a]Number in brackets indicates upper bound of behavior if it can be demonstrated that the behavior does affect pipeline operation or maintenance or promote failure

[b]Ovality which produces the yield level hoop stresses in the pipe, assuming a yield strength of 480 MPa and a wall thickness of 10 mm

3.1 Portland cement grout

The strain value of concrete, ε'_c, was taken as 0.003, and the Poisson ratio of 0.2 was used. Thang [11] at Lamar University research used a Poisson ratio of 0.18. Different researchers have used strain values ranging 0.002–0.003 [7–9]. However, the strain value of 0.003 was selected in this research and it gives a better result than lower strain values when compared with test results.

Mander, Priestley, and Park [12] suggested a confined concrete stress–strain curve using Eqs. 1 and 2. The stress–strain curve of confined concrete is shown in Fig. 4.

$$f'_{cc} = f_c + k_1 f_1 \tag{1}$$

$$\varepsilon'_{cc} = \varepsilon'_c \left(1 + k_2 \frac{f_1}{f_c}\right) \tag{2}$$

where,

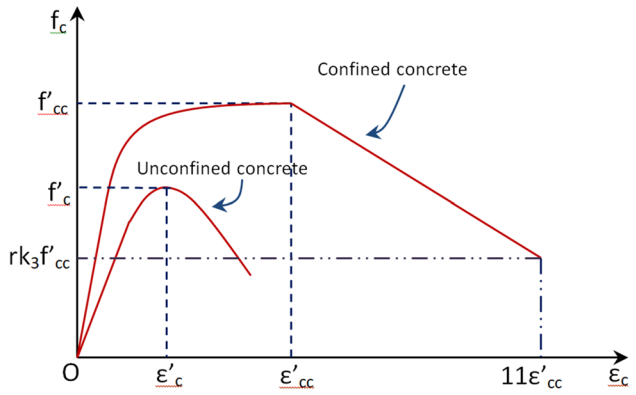

Fig. 4 Confined and unconfined concrete stress–strain curve [12]

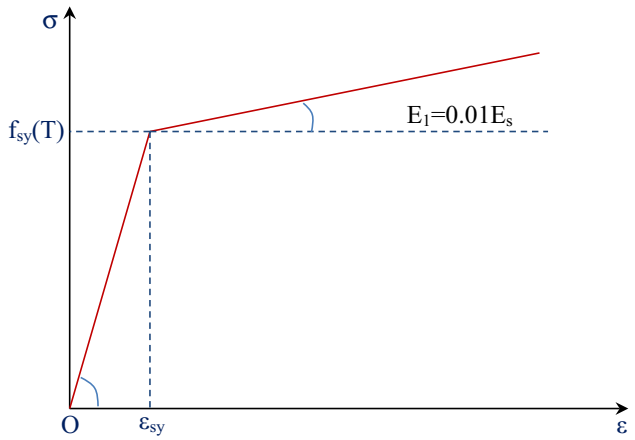

Fig. 5 Steel bilinear stress–strain curve [19]

f'$_{cc}$ = confined concrete compressive strength.

f_c = unconfined concrete cylinder compressive strength.

ε'$_{cc}$ = the confined strain corresponding to f'$_{cc}$.

The lateral pressure coefficients, k_1 and k_2, are taken as 4.1 and 20.5 respectively based on test results from Richart, Brandtzaeg, and Brown [13].

The lateral confining pressure, f_1, is given by Hu and Su [8] as:

$$f_1 = 8.525 - 0.166\left(\frac{D_o}{t_o}\right) - 0.00897\left(\frac{D_i}{t_i}\right) + 0.00125\left(\frac{D_o}{t_o}\right)^2 + 0.00246\left(\frac{D_o}{t_o}\right) \times \left(\frac{D_i}{t_i}\right) - 0.00550\left(\frac{D_i}{t_i}\right)^2 \geq 0 \quad (3)$$

where

D_o = diameter of outside tubular.

t_o = wall thickness of outside tubular.

D_i = diameter of inside tubular.

t_i = wall thickness of inside tubular.

Liang [10] also suggested that Eq. 3 should be used for steel–concrete–steel sandwich short columns. Saenz [14] suggested the nonlinear behavior of concrete using the equation:

$$f_c = \frac{E_c \varepsilon_c}{1 + (R + R_E - 2)\left(\frac{\varepsilon_c}{\varepsilon'_{cc}}\right) - (2R - 1)\left(\frac{\varepsilon_c}{\varepsilon'_{cc}}\right)^2 + R\left(\frac{\varepsilon_c}{\varepsilon'_{cc}}\right)^3} (\text{MPa}) \quad (4)$$

where $R = \frac{R_E(R_\sigma - 1)}{(R-1)^2} - \frac{1}{R_\varepsilon}, R_E = \frac{E_c \varepsilon'_{cc}}{f'_{cc}}$.

E_c = Modulus of elasticity of unconfined concrete.

ε_c = Unconfined strain corresponding to f_c.

R_E = Parameter related to the modulus of elasticity of concrete and the ratio of the confined strain ε_{cc} to the corresponding compressive strength fcc.

R_σ = Parameter in defining the stress–strain relationship of confined concrete.

Rε = Parameter in defining the stress–strain relationship of confined concrete.

R = Parameter dependent upon RE, Rσ, and Rε.

Hu and Schnobrich [15] assumed $R_\sigma = R_\varepsilon = 4$. As per ACI 318, modulus of elasticity of normal weight concrete is:

$$E_c = 4700\sqrt{f'_{cc}} (\text{MPa}) \quad (5)$$

The end point of confined concrete compressive stress on stress–strain curve beyond peak stress is taken as rk$_3$f'$_{cc}$ and the strain value at that point is 11ε$_{cc}$, where the material degradation parameter, k_3, Hu and Su [8] is given by:

$$k_3 = 1.73916 - 0.00862\left(\frac{D_o}{t_o}\right) - 0.04731\left(\frac{D_i}{t_i}\right) + 0.00036\left(\frac{D_o}{t_o}\right)^2 + 0.00134\left(\frac{D_o}{t_o}\right) \times \left(\frac{D_i}{t_i}\right) - 0.0058\left(\frac{D_i}{t_i}\right)^2 \geq 0 \quad (6)$$

The reducing factor, r, is taken as unity for concrete cube strength up to 30 MPa [16], 0.5 for 100 MPa and higher strength is used [17, 18]. The reducing factor in between can be calculated by interpolation and the method is also adopted by Pagoulatou et al. [9].

3.2 Steel materials

For steel, bilinear stress–strain curve as shown in Fig. 5 is used, adopted by Han and Huo [19].

The elastic part of the steel is calculated using equations below for the plastic region.

$$\sigma_i = E_s(T) \times \varepsilon for \varepsilon \leq \varepsilon_{sy}(T) \quad (7)$$

$$\sigma_i = f_{sy}(T) + E_1(T) \times \left(\varepsilon - \varepsilon_{sy}(T)\right) for \varepsilon > \varepsilon_{sy}(T) \quad (8)$$

where f_{sy} (T) is yield strength of the steel at a given temperature T. ε_{sy} (T) given in Eq. 9 is the corresponding strain and it can be calculated by,

$$\varepsilon_{sy}(T) = \frac{f_{sy}(T)}{E_s(T)} \quad (9)$$

In this research, the temperature is taken as room or normal temperature and hence there is no temperature effect. Modulus of elasticity, $E_s(T)$, is taken as 200,000 N/mm^2, $E_1(T)$ is taken as 0.01 Es(T), and Poisson's ratio of 0.3 is used. The modulus of elasticity and Poisson ratio used is widely accepted and used by researchers for mild carbon steel [7–9]. Normal temperature condition is used for this analysis and hence temperature does not affect the analysis results.

3.3 Steel–concrete–steel double-wall pipe analysis in air

For cement grout, the elastic and Drucker–Prager plastic properties were entered for grout material. As FE analysis performed by Pagoulatou et al. [9], the angle of friction and flow stress ratio are 20 and 0.8 respectively. The calculated grout plastic stress–strain curve using Eq. 4 was entered in Drucker–Prager hardening sub-options for compression. Elasticity of cement grout was calculated using Eq. 5. FE analysis assembly and boundary conditions are shown in Fig. 6. The purpose of this analysis is to verify FE composite pipe analysis against the test results.

Elastic and plastic material properties are used for steel. The steel plastic stress–strain curve is calculated using Eq. 8 for inner and outer tubular. Elastic property only was used for end cap, and the modulus of elasticity used is 1000 times higher than normal steel so that it does not deform and thus load is uniformly applied on the composite tube section.

For interaction properties, primary–secondary surface to surface discretization was used between steel and cement grout with steel being the primary and cement grout surface being the secondary. As the primary steel moves, the cement grout follows the steel's deformation. Lam et al. [20] used 'tangential behavior' with friction of 0.3, and 'hard contact' for 'normal behavior'. The same interaction properties are used herein. 'Hard contact' interaction minimizes the primary surface penetrates into the secondary surface. Pressure can be transmitted when in contact and separated when there is no pressure. Small friction values have issue with convergence. However, 0.3 friction value provides satisfactory results, and hence more studies were not conducted. The same primary–secondary interaction was used for end cap and composite tube with end cap being the primary and composite tube being the secondary. Large tangential behavior for friction 0.99 was used for the cap contact. The base end surface of the composite pipe was pinned. The end cap was restraint against X and Y direction. Displacement loading was applied on the end cap along negative Z axial direction.

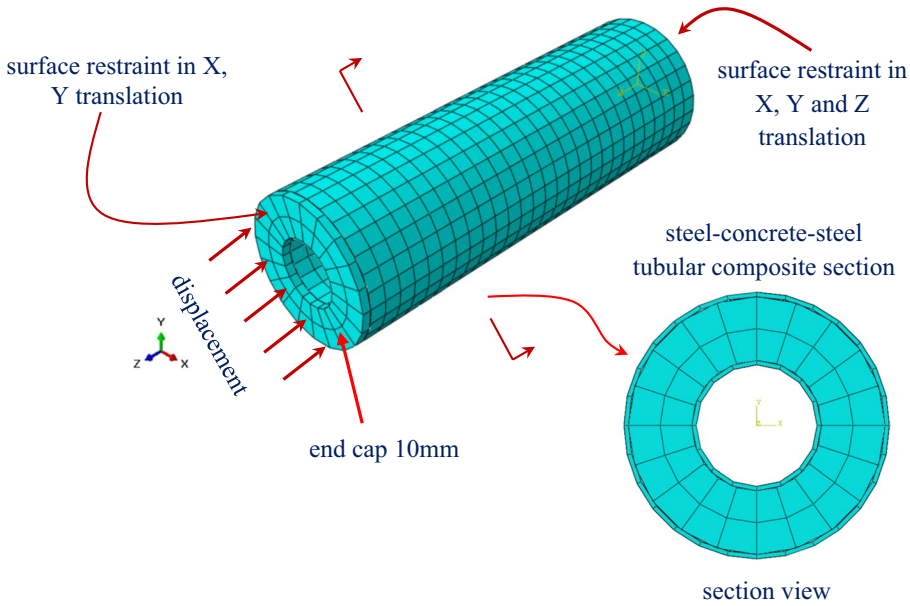

Fig. 6 FE analysis assembly and boundary conditions of steel–concrete-steel composite pipe

4 FE analysis results

4.1 Single-wall pipe in clay

A finer and coarser mesh of pipe in clay was studied. For the finer mesh model, mesh size around the pipe was 6 cm wide and 10 cm long, 16 elements around the pipe for pipe diameter 31.9 cm with thickness 1.27 cm. Pipe embedded length was 12.8 m (40 ft). Mesh size in clay model around the pipe was 20 cm. For a coarser mesh model, there were 12 elements around the pipe (10 cm) and the length of the mesh size was 20 cm. Mesh size in clay model around the pipe was 25 cm. C3D8R 8-node linear brick elements were used. Lateral displacement was applied at the pipe top. FE analyses for two different mesh sizes were documented using cap plasticity of clay model and the results are plotted in Fig. 7.

It can be seen from the lateral force vs displacement plot that finer mesh and coarser mesh sizes do not have much difference in analysis results. This is also the same for stresses – both coarse and finer mesh sizes showing comparable analysis results. So, the analysis was further performed using the finer mesh sizes for both cap plasticity model and Marshall's rigid plastic model. The analysis results of cap plasticity, Marshall plastic model, and Matlock's test are plotted in Fig. 8.

Beyond 20 cm pipe lateral displacement, FE analysis with Marshall's plastic model appears to have slightly larger displacement capacity compared to the test result as the applied load increases. The lateral load capacity is 40% larger than the Matlock's test at 10 cm pipe top displacement. The difference in capacity appeared to start to deviate when the clay's stresses reached elasticity limit. The clay cap plasticity model appears to be almost perfectly matching the test result. The initial stiffness is

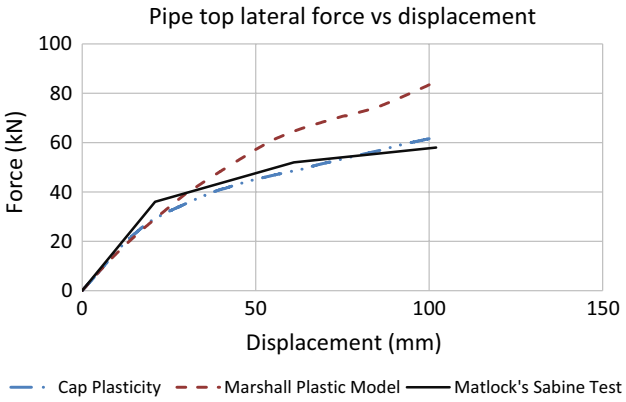

Fig. 8 Analysis results of cap plasticity model and Marshall's plastic model

well predicted with no imperfection included. However, the slight difference results could also be due to the clay modulus of elasticity ranges of choices, and stress–strain curve model of the plastic soil. One of the reasons Marshall's clay has a much larger lateral capacity was because the strain values used were small and this strain values represent stiff clay in several research papers and books. On the other hand, the cap model used soft clay strain values which represent the actual strain value in the soft clay test.

4.2 Analysis results of steel–concrete–steel double-wall pipe in air

Qualitative comparison of FE results and Test failure image in Fig. 9 shows local buckling failure occurs at a region along the composite column. In this study, the same strength of cement was used for all three analyses. For smaller steel tube outer diameter with 180 mm, local buckling failure occurs near the base with pinned fixity.

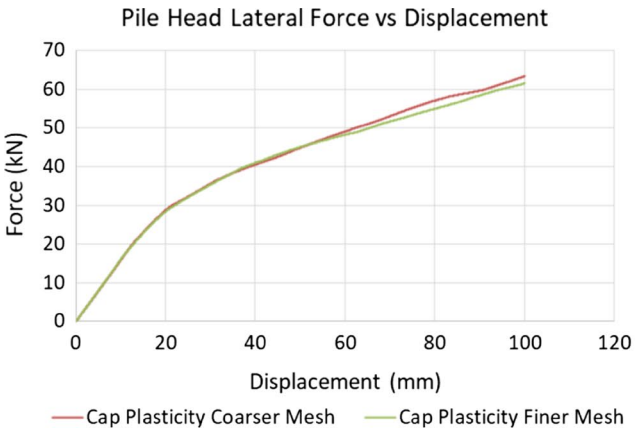

Fig. 7 Force–displacement analysis results of different mesh sizes

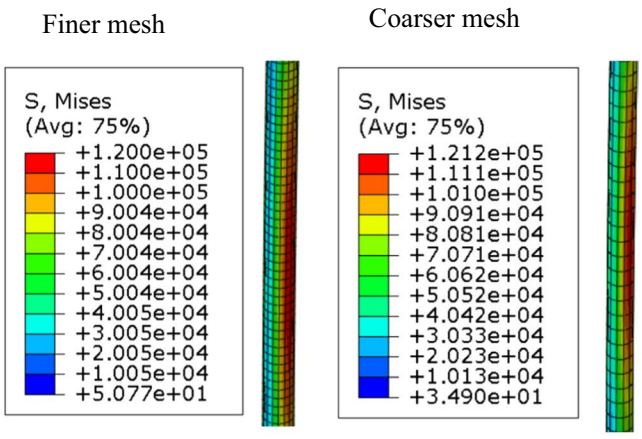

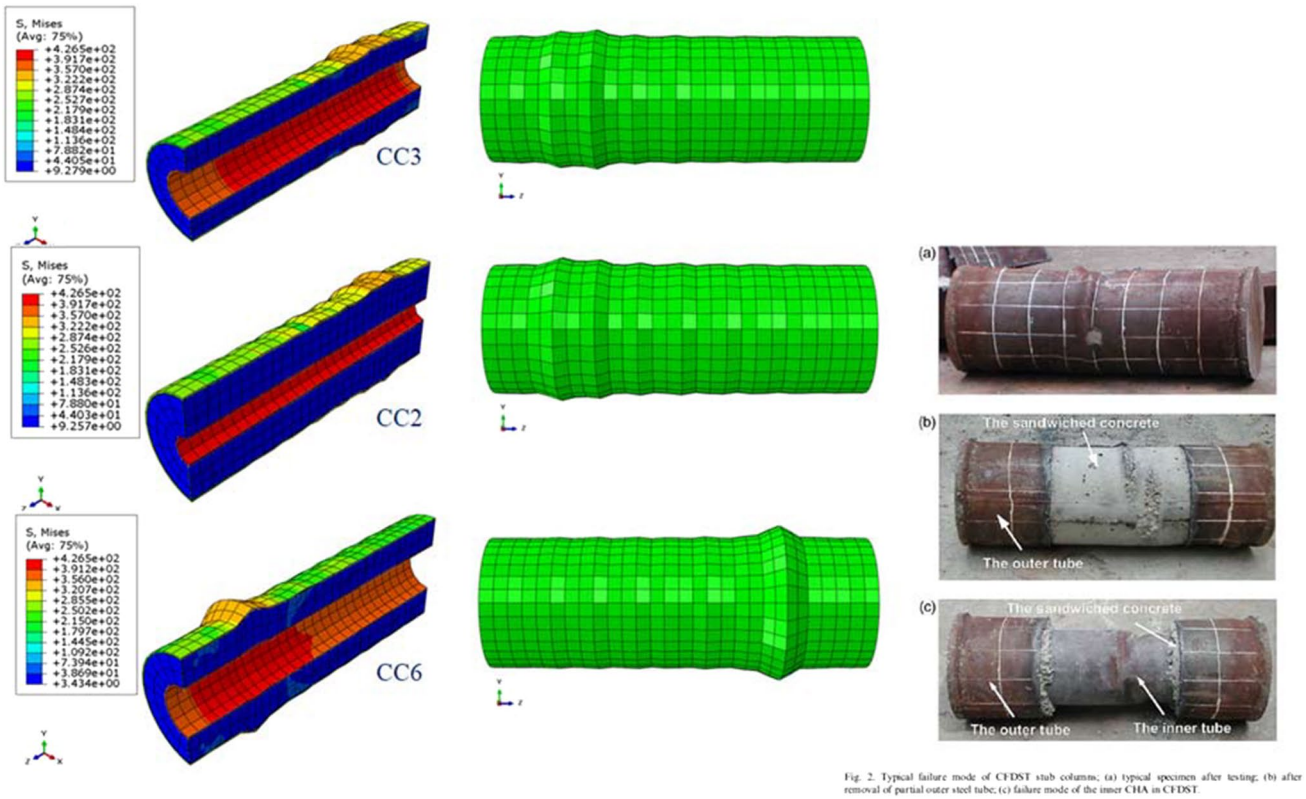

Fig. 2. Typical failure mode of CFDST stub columns; (a) typical specimen after testing; (b) after removal of partial outer steel tube; (c) failure mode of the inner CHA in CFDST

Fig. 9 FE analysis results comparison: Thang et al. [2] vs Tao et al. [7]

CC2a has thicker grout 63 mm compared to CC3a with thickness 43 mm; however, the location of failure for both composite tubes is the same and have identical failure. For a larger tubular diameter such as CC6a with outer diameter 240 mm and annulus 60 mm, local buckling failure is near end cap loading. The tubular thicknesses are 3 mm. Overall, failure patterns for the composite tube are the same regardless of change in steel tubes diameter with larger tube diameter appears to have lesser buckling failure compared to the smaller composite tube diameter. Both steel and cement grout materials have almost reached their ultimate strength as shown in von Mises stresses in Fig. 9. Comparisons between the quantitative results of three FE models (solid lines) and experiment test results (dashed lines) are presented in Fig. 10. It can be seen that three solid curves (FE models) and three dashed curves (experiments) are fairly close in trends. This simulation was performed to verify FE analysis results of the composite pipe in line with experiment test results.

FE analysis results are closely matching with test results. It can also be deduced that load capacity reduced much faster for a larger diameter with composite tube. CC2a and CC3a analysis result shows load reduces slowly with increase in the strain, whereas load reduction is more rapid in larger diameter CC6a.

4.3 Single-wall pipe analysis results in clay

Two different pipe Sects. $50.8\varnothing \times 2.54$ cm and $50.8\varnothing \times 1.27$ cm were embedded in solid model which represents clay properties. This represents a pile foundation of fixed offshore structure or half of a buried seafloor pipeline. The results were compared against Marshall [26] published results. In addition to the strains, stresses, and lateral displacements, ovalizing of the pipe was also observed and compared against acceptable industry limits. From the research, it was found that pipeline has more stringent governing factors compared to a pile foundation of fixed structure such as jacket structure. It is because pipeline requires to meet strict industry standards whereas pile is mainly dependent on the allowable stresses.

Figure 11 shows force–deflection of the two pipes. The thicker pipe being higher stiffness is able to take higher load. These results shown are the final von Mises steel stress and soil mesh deformation. These results are at the end of the analysis, where failure of the pipes have occurred.

Figure 12 shows progressive ovalization at the maximum bending point. This is set to ensure that the pipeline remains piggable. This limit is reached at a displacement of 20 cm for the thinner pipe, and 52 cm for the thicker pipe, or 40 cm and 104 cm for the pipeline at a fault. The

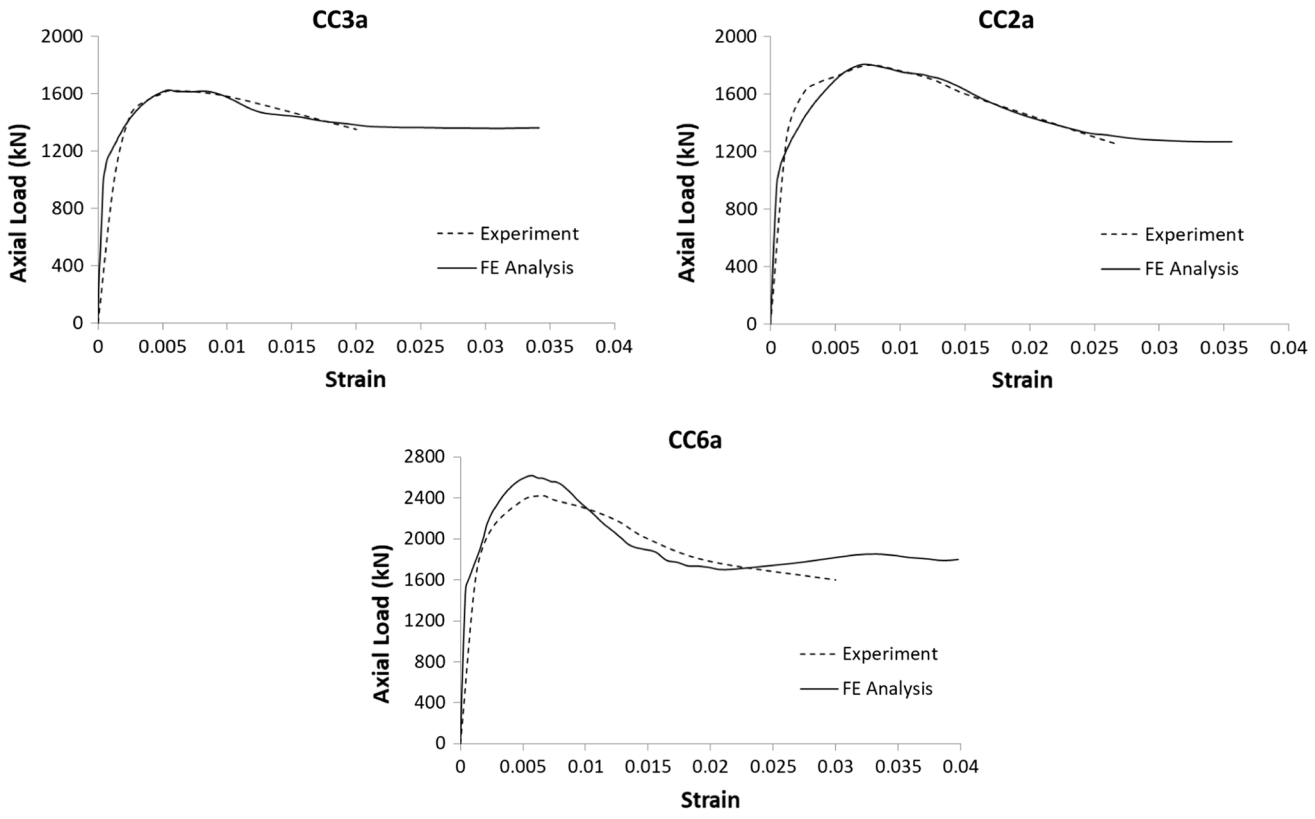

Fig. 10 Axial load-strain FE analysis results and test results plot

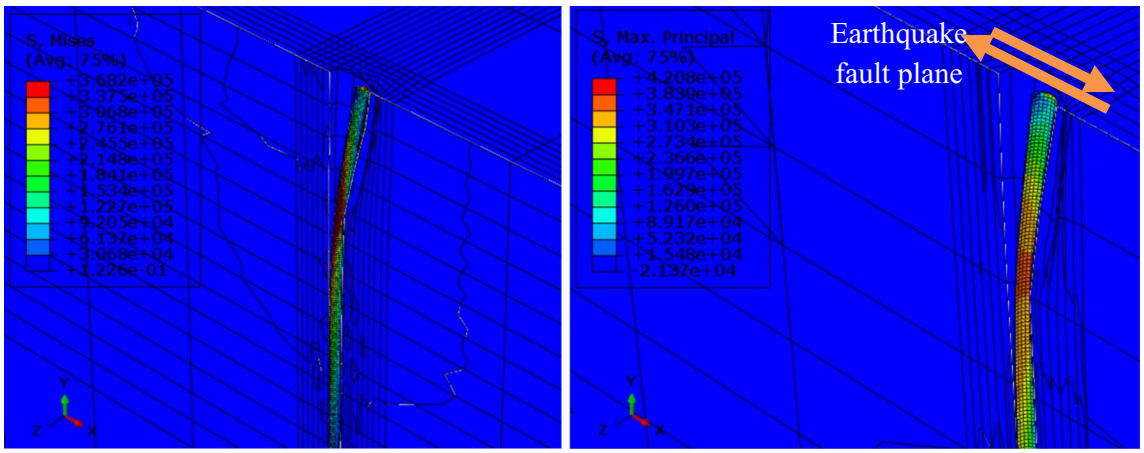

50.8∅x2.54 cm Pipe
Pile head displacement 104cm

50.8∅x1.27 cm Pipe
Pile head displacement 80cm

Fig. 11 Steel stress and soil mesh deformation

pigging device is shown in the pipe and it appears up to 6% pipe ovality is acceptable. At this deformation point, the stress was in early plastic stage with 366 MPa for the higher and thicker pipe, and strain was 0.0006%. Hence, ovalization is the governing factor for single-wall pipe ductility. The ovality was measured manually and depending on the mesh size of the tubular the nearest ovality available from the targeted value of 3% was 3.07%. Hence, to be conservative, an ovality larger than 3% was selected instead of the smaller ovality.

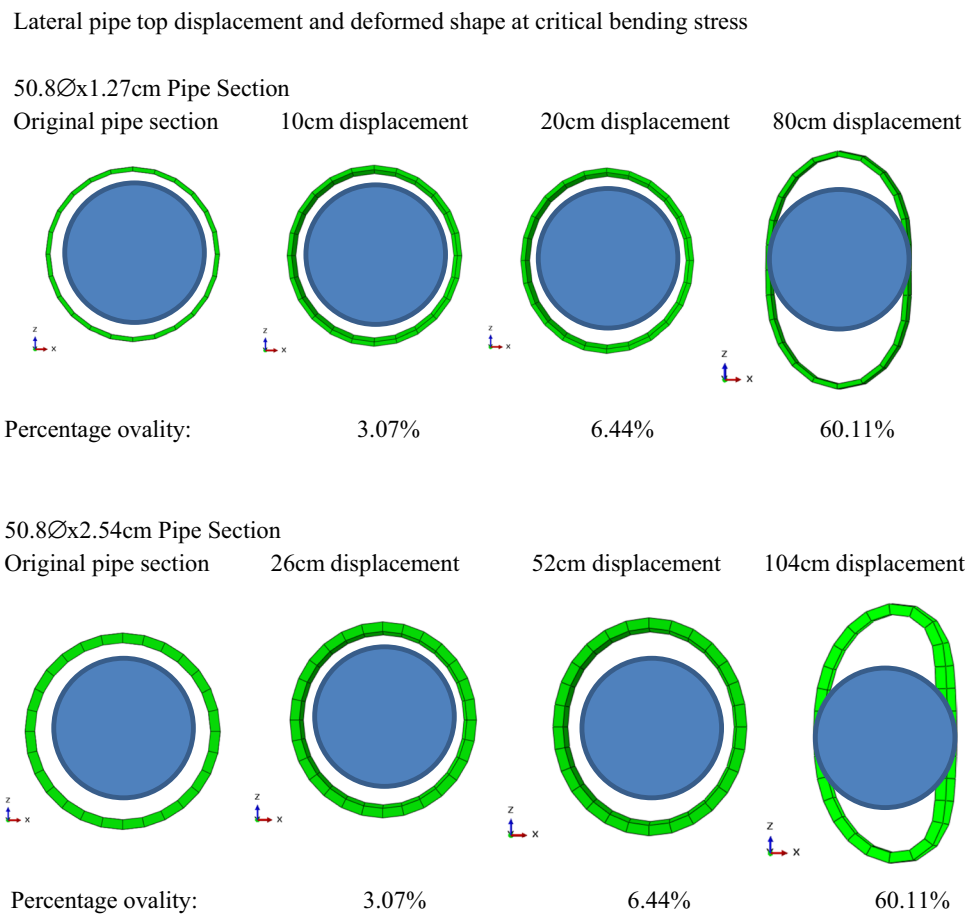

Fig. 12 Progressive ovalization with pigging device in the pipe by Thang et al. [2]

4.4 SPS double-wall composite pipeline analysis results in clay

Double-wall composite pipe 60.96 cm × 1.27 cm (24in × 0.5in) and 50.8 cm × 1.27 cm (20in × 0.5in) was also analyzed using coarser mesh than the single-wall pipe for a better analysis convergence. The elements around the circumference used were 16 for single-wall pipe, whereas 28 elements around the pipe were used for single-wall pipe. The steel and polymer interface was treated as perfectly bonded, and they are tied in the model. The polymer material was modeled as elastic with a modulus of elasticity of 20,000 MPa as the detailed material's plastic stress–strain properties are not yet available at this stage. The analysis was performed in clay the same as single-wall pipe. The von Mises stress, principal strain and deflection of the pipe are shown in Fig. 13. The stress in steel was 378.5 MPa and the strain was 1.43%. The half pipe deflection was 2.134 m. The total offset when the two composite pipes connected was 4.27 m. Single-wall pipe with thickness 6.35 cm which is the same as total thickness of SPS section was also analyzed. The strain was limited at 2% and at this stage, and the total pipeline deflection was 4.16 m. The pipe ovality was 5.3%, slightly less than the ovality limit of 6%. The steel section was in plastic stage at this ovality.

4.5 Comparison of SPS double-wall composite pipe and single-wall pipe in air

This work compares 5.08 cm (2in) thick single-wall pipe and 5.08 cm (2in) overall thickness of composite pipe. The beam length used was 3.6127 m. The single-wall pipe was 60.96 cm × 5.08 cm (24 × 2in). Double-wall composite pipe is 60.96 cm × 1.27 cm (24in × 0.5in) and 53.34 cm × 1.27 cm (21in × 0.5in), the annulus 2.54 cm (1in) thick was grouted with polymer. One end was pinned, and the other end of the pipe was roller support. The interface between steel and polymer was tied. Rotation about x-axis was applied at both ends. Single-wall pipe failed by buckling, and wrinkles were formed at mid-length. However, such failure did not occur in double-wall composite pipe as shown in Fig. 14. Strain at 2% was observed as suggested by the industry code, such as DNV-OS-F101 [31] and ASCE [32]. Double-wall composite pipe reached 2% strain in the steel at rotation angle of 11 degree. However, the rotation angle of single-wall pipe was 9 degrees at this point. The single-wall pipe also experienced higher stress

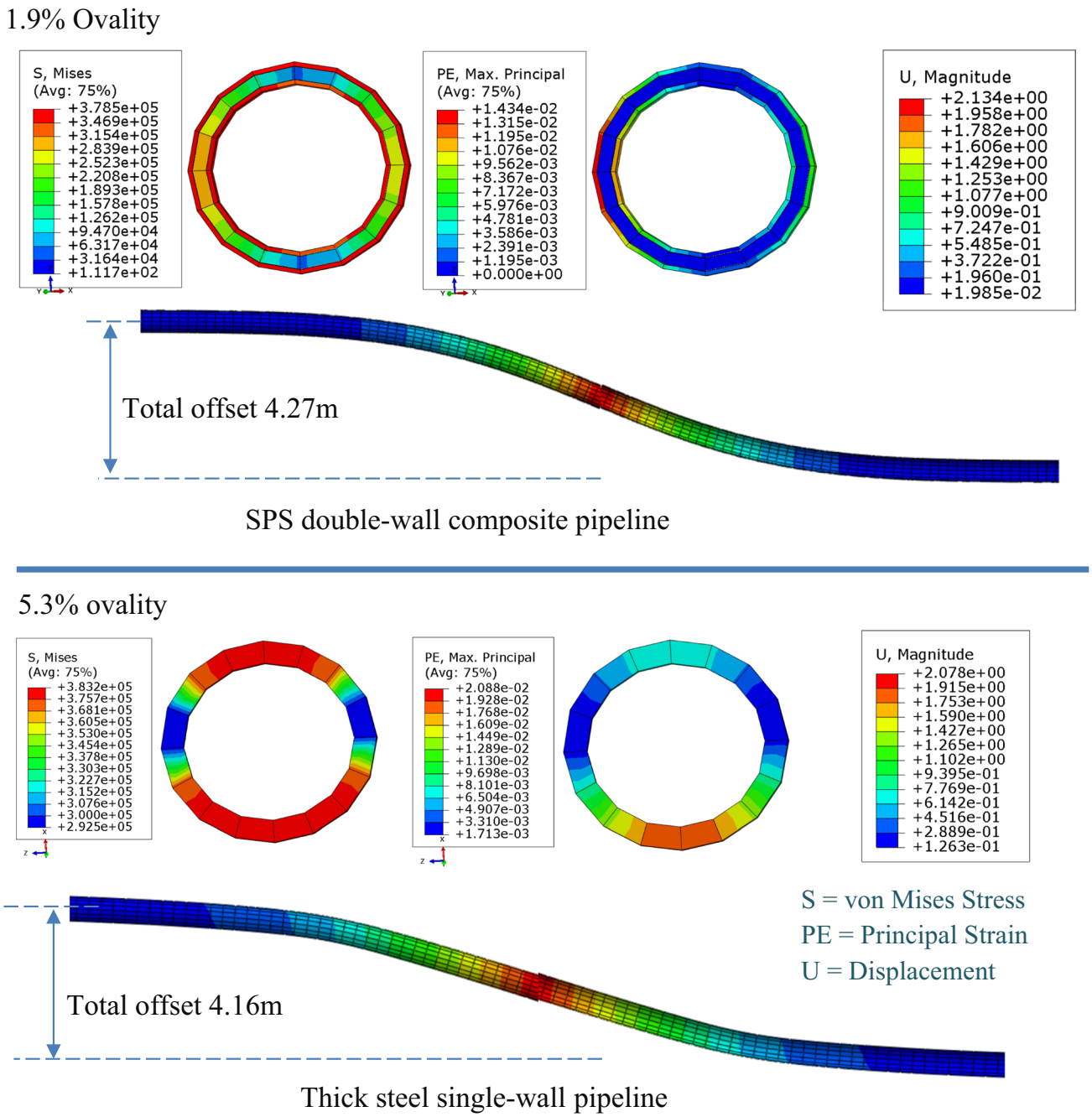

Fig. 13 Analysis results of double-wall composite pipe in clay

with 396 MPa. The double-wall composite pipe experienced slightly lower stress with 383 MPa. Although these may be acceptable, the single-wall pipe ovality was 9% and this is way over acceptable limit of 6%. The double-wall composite pipe experienced very small ovality of just 0.52%. Therefore, it can be seen that the double-wall composite pipe with polymer grout significantly improves the pipe ovalization. Figure 14 shows 60.96 cm × 5.08 cm (24in × 2in) single-wall, and double-wall composite pipes bending in air analysis results comparison. Wrinkle and buckling failures are shown in finer meshed tubular pipe but these characteristics are not shown in coarser meshed pipe.

4.6 Imperfect SPS double-wall composite pipe analysis in air

This test was performed to see if imperfection such as girth weld in the steel pipe has effect on the analysis results. The

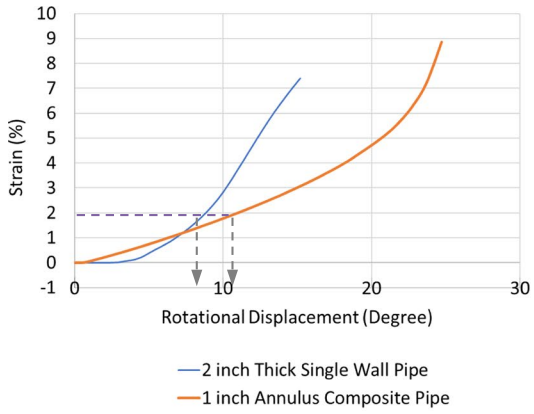

(a) Strain – rotational displacement capacity

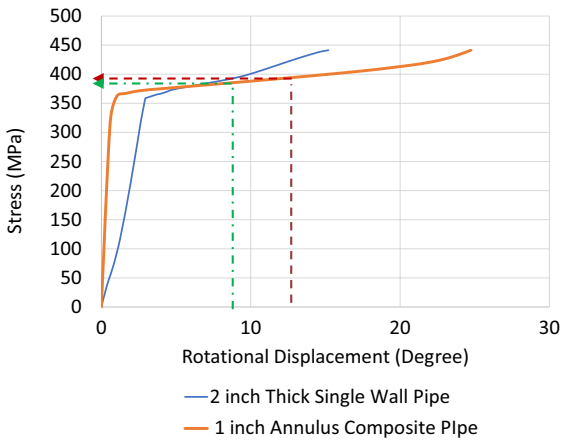

(b) Stress – rotation displacement capacity

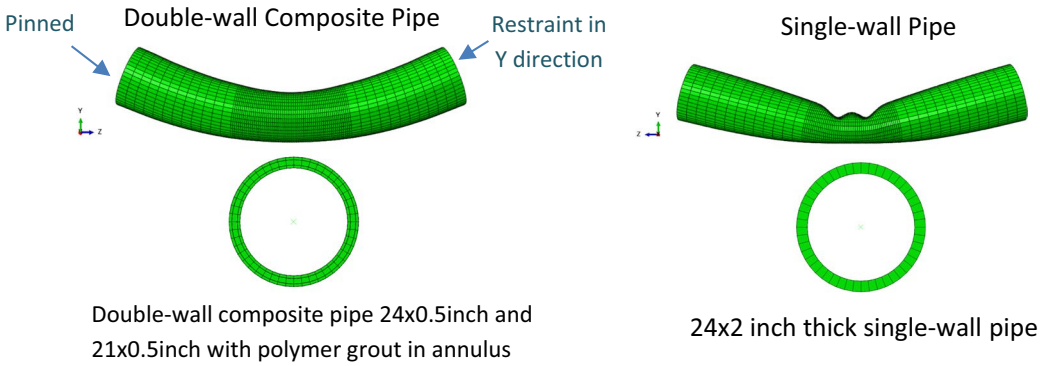

(c) Beams deformed shape at ultimate failure

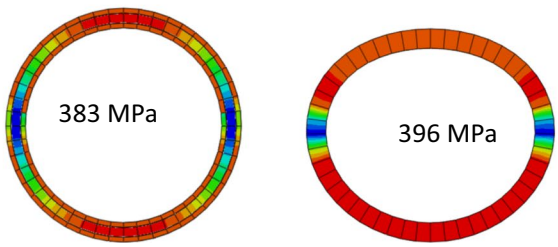

(d) Deformed single-wall and double-wall composite pipe at a strain of 2%.

Fig. 14 Bending of a 60.96 cm × 5.08 cm single-wall and double-wall composite pipes in air

beam length was 3.6127 m long. Two vertical displacement downward loads were being applied at 1.20 m from each support. Mesh size was finer, 2 cm at mid-region of the beam length, and coarser 10 cm between the load and end points. There were 48 elements around the pipe. Mesh element types were C3D8R, an 8-node linear brick, reduced integration, hourglass control. The beam assembly and boundary conditions are shown in Fig. 15. The polymer grout elastic modulus of 200 MPa, 2000 MPa, 20,000 MPa were tested for both imperfect (with weld) and intact (without weld) composite pipes. Thickness/8 center line offset used for the weld is recommended by API 579-1/ASME FFS-1 [34].

4.6.1 Imperfect double-wall composite pipe analysis results

Force–displacement analysis results of imperfect composite pipe and intact composite pipe are shown in Fig. 16. From the force–displacement plot, the intact and imperfect

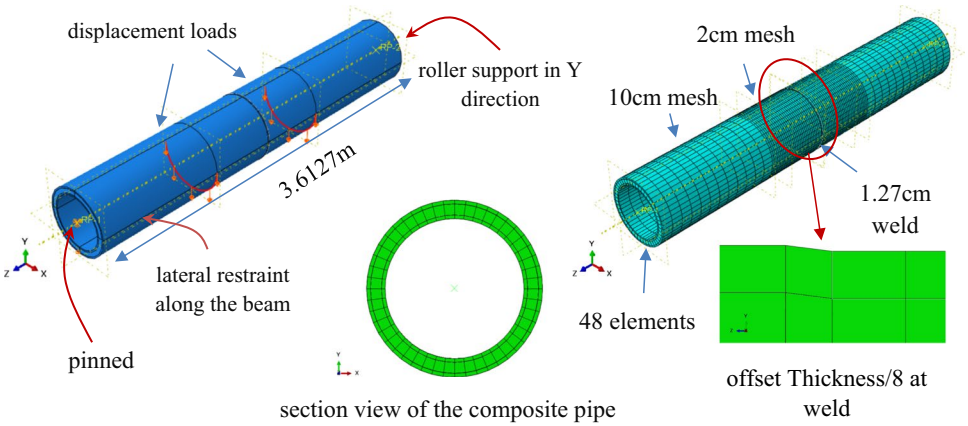

Fig. 15 Imperfect bonded composite pipe

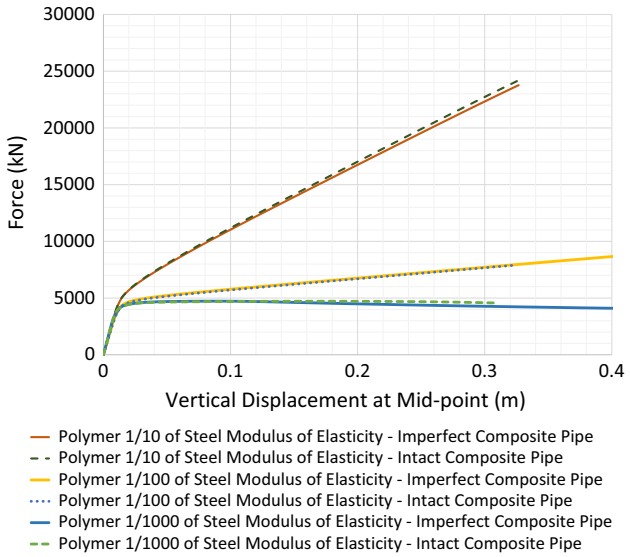

Fig. 16 Load capacities comparison of the bonded imperfect and perfect composite pipes

composite pipe analysis results have negligible differences for all the 3 different polymer stiffness.

4.6.2 Issues with double-wall SPS sandwich pipe

Wrinkles were found in steel pipes when polymer with low modulus of elasticity of polymer was used. Wrinkles were also appeared when there is no bond between the steel and polymer which interfaces are the same as steel–concrete–steel axial load test as explained earlier. Figure 17 shows wrinkles in low polymer stiffness and unbonded interface between the steel polymers. These wrinkles are highly undesirable in pipeline.

5 Discussion

Verifications FE analysis results show the parameters used for analysis are correct, FE analysis results are correct, and hence the analysis results are acceptable. Evidence can be found in FE analysis results for laterally loaded single-wall pipe in clay and double-wall steel–concrete–steel. Thus,

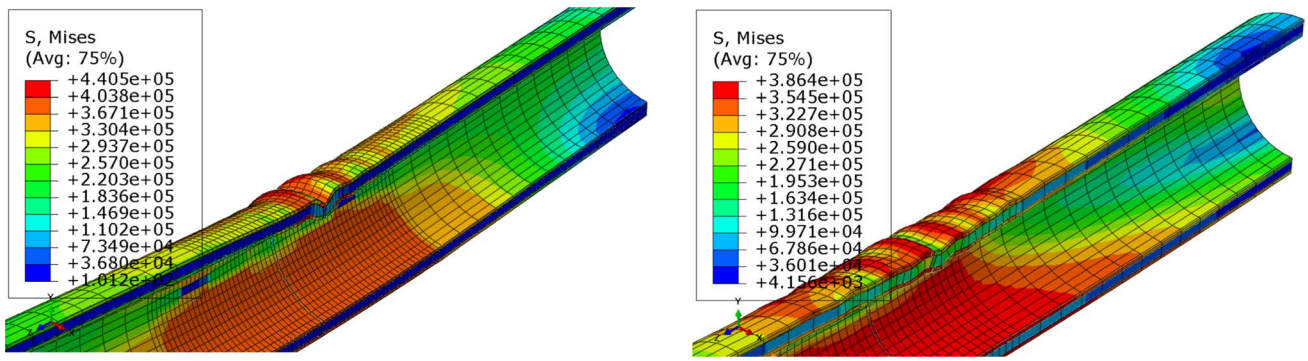

soft polymer with modulus of elasticity 200 MPa

unbonded interface between steel and polymer

Fig. 17 Wrinkles in composite pipes with soft polymer and no bonding between the steel polymer interfaces

further FE analysis performed for the SPS composite pipe results are reliable.

In single-wall pipeline, ovality governs the pipeline design and wrinkles are observed at maximum bending locations. When SPS double-wall composite pipe is introduced, the ovality and wrinkle issue no longer exist and the composite pipe has larger deformation capacity to accommodate offsets due to earthquake loads. For example, the SPS sandwich pipeline could deflect 4.27 m (14 ft) without showing any sign of failure. At this point of deflection, the inner pipe ovality was 1.9% and the maximum strain was 1.43%. The steel section plasticity at this point was 86%. The stresses and strain have also not failed. So, it can be observed that the composite pipe will survive without any damage where pipeline experiences offset of 4 m in earthquake fault zone. At this deformation, the thick 6.35 cm single-wall pipe has already reached a strain value of 2%. In addition, such thick and heavy pipe with wrinkle prone is not practical to use for pipeline. Marshall [26] predicted this to be 2.3 m (7.8ft) offset with strain 6.4% when using the double-wall composite pipe.

From simply supported beam analysis in air, the effect of weld on just the outer steel has no significant impact on the analysis results. Thang et al. [25] studied the welding effect of a double-wall composite pipe on the outer and inner pipes and found that due to the weld the strain increases by 37%, ovality increases by 54%, and the stress increases by 3.3%. More detailed imperfection effect will be investigated in future studies.

Analysis results comparison for 5.08 cm (2 in) thick pipe in air in Fig. 14 earlier, the single-wall and SPS double-wall composite pipes analysis results show that the SPS composite pipe brings significant improvement from using thick single-wall pipe. Wrinkles and local buckling found in single-wall pipe are no longer present in the double-wall composite pipe. For the same angle of rotation, double-wall pipe has ovality of just 0.52% whereas the single-wall pipe has ovality of over 9% with slightly higher stress. Therefore, clearly the analysis result shows that using double-wall SPS composite pipe in offshore pipeline has huge benefits.

Comparing the pipeline in clay for single-wall and double-wall SPS composite pipeline for equal thickness in Fig. 13 earlier, it is clear that the composite pipe defeats single-wall pipe in all areas for the same pipeline deflection. However, one should also note that there need to be bonding between the steel and polymer, and also the polymer should be sufficiently stiff. Analysis in this research found polymer 100 times less than the steel's modulus of elasticity eliminates wrinkles in the steel. So, it was found that polymer modulus of elasticity of 2000 MPa may also be effective. The stiffness of polymer is to be decided based upon the availability from the industries.

6 Conclusion

From the research work, FE analysis results and test results match for the steel–concrete–steel double-wall composite pipe, and laterally loaded single-wall pipe in clay. Double-wall SPS composite pipe with polymer grout has significant improvement in terms of ductility with sufficiently stiff polymer and good bond between polymer and steel.

The SPS double-wall composite pipe has ability to deflect larger than the single-wall pipe. It has no ovality issue and has no wrinkles when a sufficiently stiff polymer is used and when there is a bond between the polymer and the steel. The strain developed is also relatively small compared to that of single-wall pipe. In offshore or onshore pipeline, ovality and strain are always a concern, and this new SPS double-wall composite pipe is perfectly suitable for such applications. In addition, with two thin double-wall pipes with annulus grouted with polymer, the composite section will have a lighter weight than the same thickness of single-wall steel pipe.

Apart from ductility, ovality, strain and stresses improvement, there may be several more benefits using double-wall composite pipe section. The composite pipe performance in areas, such as pressure, corrosion, impact, fatigue and fracture, will be investigated in future studies.

Declarations

Conflict of interest The authors declare that they have no conflict of interest.

Ethical approval The authors state that the research was conducted according to ethical standards.

References

1. Broms BB. Lateral resistance of piles in cohesive. J Soil Mech Found Div. 1964;90:3–123.
2. Thang, V., Marshall, P.W., Hui, D. (2020). Buried Seafloor Pipeline Crossing a Fault. Global Oceans 2020: Singapore–US Gulf Coast Conference.
3. Vasilikis D, Karamanos SA. Mechanical behavior and wrinking of lined pipes. Int J Solids Struct. 2012;49:3432–46. https://doi.org/10.1016/j.ijsolstr.2012.07.023.
4. Papadaki CI, Chatzopoulou G, Sarvanis GC, Karamanos SA. Buckling of internally-pressurized spiral-welded steel pipes under bending. Int J Press Vessels Pip. 2018;165:270–85. https://doi.org/10.1016/j.ijpvp.2018.07.006.
5. Uckan E, Akbas B, Shen J, Rou W, Paolacci F, O'Rourke M. A simplified analysis model for determining the seismic response of buried steel pipes at a strike-slip fault crossings. Soil Dyn Earthq Eng. 2015;75:55–65. https://doi.org/10.1016/j.soildyn.2015.03.001.

6. Marshall PW, Gates WE, Nahin. (May 1977). Analytical Methods for Determining the Ultimate Earthquake Resistance of Fixed Offshore Structures, Proc Offshore Tech Conf, OTC 2751.
7. Tao Z, Han L-H, Zhao X-L. Behaviour of concrete-filled double skin (CHS inner and CHS outer) steel tubular stub columns and beam-columns. J Constr Steel Res. 2004;60:1129–58. https://doi.org/10.1016/j.jcsr.2003.11.008.
8. Hu H-T, Su F-C. Nonlinear analysis of short concrete-filled double skin tube columns subjected to axial compressive forces. Mar Struct. 2011;24:319–37. https://doi.org/10.1016/j.marstruc.2011.05.001.
9. Pagoulatou M, Sheehan T, Dai X, Lam D. Finite element analysis on the capacity of circular concrete-filled double-skin steel tubular (CFDST) stub columns. Eng Struct. 2014;72:102–12. https://doi.org/10.1016/j.engstruct.2014.04.039.
10. Liang QQ. Nonlinear analysis of circular double-skin concrete-filled steel tubular columns under axial compression. Eng Struct. 2017;131:639–50. https://doi.org/10.1016/j.engstruct.2016.10.019.
11. Thang, V. (2014). Studded Bond Enhancement for SCS Sandwich Shells. M.S. Thesis. Lamar University.
12. Mander JB, Priestley MJ, Park R. Theoretical stress-strain model for confined concrete. J Struct Eng. 1988;114(8):1804–26.
13. Richart FE, Brandtzaeg A, Brown RL (1928). A study of the failure of concrete under combined compressive stresses, Bulletin No. 185. Champaign: University of Illinois, Engineering Experiment Station.
14. Saenz L. Discussion of paper "Equation for Stress-Strain Curve of Concrete" by Desai, P. and Krishnan S. J Am Concr Inst. 1964;61:1229–35.
15. Hu H, Schnobrich W. Constitutive modeling of concrete by using nonassociated plasticity. Mater Civil Eng. 1989;1(4):199–216.
16. Giakoumelis G, Lam D. Axial capacity of circular concrete-filled tube columns. J Constr Steel Res. 2004;60:1049–68. https://doi.org/10.1016/j.jcsr.2003.10.001.
17. Mursi M, Uy B. Strength of concrete fillled steel box columns incorporating interaction buckling. J Struct Eng ASCE. 2003;129(5):626–39.
18. Tomii, M. (1991). Ductile and strong columns composed of steel tube, infilled concrete and longitudinal steel bars. Proceedings of the 3rd international Conference on Steel-Concrete Composite Structures. Fukuoka: Association of Steel-Concrete Structures.
19. Han L-H, Huo J-s. Concrete-filled hollow structural steel columns after exposure to ISO-834 fire standard. J Struct Eng. 2003;129:68–78.
20. Lam D, Dai X, Han L, Ren Q, Li W. Behaviour of inclined, tapered and STS square CFST stub columns subjected to axial load. Thin-WalledStructures. 2012;54:94–105. https://doi.org/10.1016/j.tws.2012.02.010.
21. Thang V, Marshall PW, Brake NA, Adam F. Studded bond enhancement for steel-concrete-steel sandwich shells. Ocean Eng J. 2016;124:32–41.
22. Matlock, H. (1970). Correlation for Design of Laterally Loaded Piles in Soft Clay. Offshore Technology Conference.
23. ABAQUS/CAE User's Guide. (2014). Abaqus 6.14.
24. Helwany S. Applied Soil Mechanics with ABAQUS Applications. John Wiley; 2007.
25. Thang V, Hui D, Zhou J, Marshall PW. Failures prevention of seafloor composite pipelines using enhanced strain-based design. Rev Adv Mater Sci. 2022;2022(61):1–16. https://www.degruyter.com/document/doi/10.1515/rams-2022-0035/pdf.
26. Marshall. P.W. (2004). Enhanced Strain-Based Design of Tubular Members., Structural Stability Research Council, Proceedings.
27. API RP2A 1111. (1999). Design, Construction, Operation, and Maintenance of Offshore Hydrocarbon Pipelines. American Petroleum Institute.
28. API-5L. (2013). API Specificaiton 5L, Specification for Line Pipe. American Petroleum.
29. Bai Q, Bai Y. (2014). Subsea Pipeline Design, Analysis, and Installation. Gulf Professional Publishing.
30. Mohr, W. (2003). Strain-Based Design of Pipeline. Submitted to US Dept. of Interior, Minerals Management Services and US Dept. of Transportation, Research and Special Programs Administration.
31. DNV-OS-F101. (2013). Submarine Pipeline Systems. Det Norske Veritas.
32. ASCE. (2005). Guideline for the Design of Buried Steel Pipe. Americal Society of Civil Engineers.
33. Liu B, Liu XJ, Zhang H. Strain-based design criteria of pipelines. J Loss Prev Process Ind. 2009;22:884–8. https://doi.org/10.1016/j.jlp.2009.07.010.
34. API 579–1/ASME FFS-1. (2007). Fitness-For-Service. The American Society of Mechanical Engineers.